PAPER

Electrochemically-gated delivery of analyte bands in microfluidic devices using bipolar electrodes†

Karen Scida, Eoin Sheridan‡ and Richard M. Crooks*

A method for controlling enrichment, separation, and delivery of analytes into different secondary microchannels using simple microfluidic architecture is described. The approach, which is based on bipolar electrochemistry, requires only easily fabricated electrodes and a low-voltage DC power supply: no pumps or valves are necessary. Upon application of a voltage between two driving electrodes, passive bipolar electrodes (BPEs) are activated that result in formation of a local electric field gradient. This gradient leads to separation and enrichment of a pair of fluorescent analytes within a primary microfluidic channel. Subsequently, other passive BPEs can be activated to deliver the enriched tracers to separate secondary microchannels. The principles and performance underpinning the method are described.

Introduction

In microfluidic-based sensing and separation applications, the analytes of interest are often present at low concentrations, in small volumes, and contained in mixtures. Accordingly, methods are usually required to both separate and enrich the analytes prior to detection. Simplifying these tasks, while simultaneously reducing analysis time and minimizing analyte loss, are therefore important goals. In the present manuscript, we describe a new methodology that addresses these points.

A number of techniques have been developed to target fluid and analyte handling in microfluidic devices. The most popular of these involve application of external forces such as pressure (*e.g.*, valves and pumps),[1,2] electric fields (*e.g.*, dielectrophoresis, electrophoresis, and electrowetting),[3–5] magnetic fields,[6] optical effects (*e.g.*, heating),[7] capillary effects (*e.g.*, surface tension gradients),[8,9] and sound (*e.g.*, acoustofluidics).[10] In some cases, two or more of the approaches mentioned above are combined for this purpose.

Department of Chemistry and Biochemistry, Center for Electrochemistry, Center for Nano- and Molecular Science and Technology, The University of Texas at Austin, 1 University Station, A5300, Austin, TX 78712-0165, USA.
E-mail: crooks@cm.utexas.edu; Tel: +1 512-475-8674

† Electronic supplementary information (ESI) available: Two movies showing the enrichment, separation, and controlled delivery using the principal and alternative BPE configurations represented by Fig. 3 and 5, respectively; a description of the fluorescence filters used to obtain images; an explanation for the contribution of background fluorescence in Fig. 3 and 5; fluorescence micrographs showing the contribution of background fluorescence at short and long enrichment times; unedited fluorescence micrographs corresponding to Fig. 3 and 5, which were used to measure the EFs; unedited fluorescence micrographs used to measure the extent of leakage of the dyes into the gated secondary microchannels for Movies S1 and S2; and calibration curves used to calculate the EFs for both dyes. See DOI: 10.1039/c3lc50321f

‡ Present address: School of Mathematics and Physics, University of Queensland, Brisbane, St Lucia, Queensland 4072, Australia.

For instance, Liu *et al.* developed a method for the separation of analytes in a two-dimensional Y-shaped microfluidic device.[11] By applying a potential and pressure-driven flow (PDF), charged analytes were separated based on their electrophoretic mobilities and then guided into different channels. Counter-flow gradient focusing techniques (CFGF),[12] such as electric field gradient focusing (EFGF), have also proven successful for directing analytes in microfluidic systems.[13–15] CFGF methods rely on balancing the forces of electrophoretic migration and convection to simultaneously enrich and separate analytes.[16–18] As such, EFGF has been widely used in the area of protein analysis.[16,19–21] In addition, bipolar electrochemistry (also a part of the CFGF family of techniques) can be used for controlling the motion of small objects. For example Bouffier and Kuhn,[22] developed a bipolar electrochemical valve fueled by the production of H_2 gas *via* water reduction at the bipolar electrode (BPE). When enough gas was stored on one side of the BPE, the valve was lifted upwards. As soon as the gas was released the valve could return to its initial position.

In the present report, we describe a method for controlled transport and delivery of charged analytes in a bipolar microelectrochemical device[23,24] without using valves, pumps, or complicated circuitry. The approach is illustrated in Fig. 1. Here, an active BPE acts like a gate that balances the electrokinetic and convective forces acting on a charged analyte, thereby preventing it from passing into either of the microchannels on the left side of the device shown in Fig. 1a. However, when the black gate is opened and the red gate is closed (Fig. 1b), transport of the analyte is dominated by convection, rather than being balanced by migration, and the analyte is allowed to pass through the black gate and into the upper microchannel. Likewise, when the red gate is opened and the orange gate closed, the second analyte passes into the
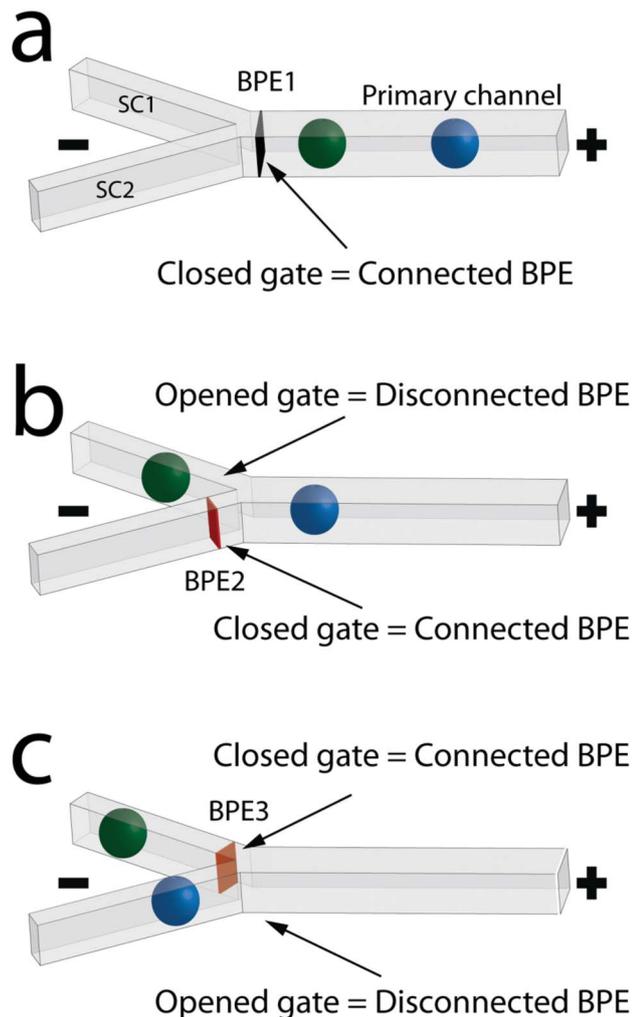
Fig. 1 Schematic diagrams illustrating the electrochemical-gating process. An active BPE is represented as a colored gate, while an inactive BPE is represented as a microchannel with no gate. The color of the gates in this figure match those of the active BPEs in Fig. 2d and Fig. 3.

lower microchannel (Fig. 1c). The key finding is that properly arranged BPEs,[23,24] along with a single DC power supply, can be used to separate and enrich charged analytes, and then direct the enriched bands into separate receiving channels.

Experimental section

Chemicals

The two fluorescent analytes used in this study were 4,4-difluoro-1,3,5,7,8-pentamethyl-4-bora-3a,4a-diaza-s-indacene-2,6-disulfonic acid, disodium salt (BODIPY^{2-}, Invitrogen Corp., Carlsbad, CA) and 8-methoxypyrene-1,3,6-trisulfonic acid (MPTS^{3-}, AnaSpec, San Jose, CA). Poly(dimethylsiloxane) (PDMS) was prepared using a silicone elastomer-to-curing-agent ratio of 10 : 1 (Sylgard 184 elastomer kit) obtained from K. R. Anderson, Inc. (Morgan Hill, CA). Au-coated glass slides

(100 nm thick, no adhesion layer) were purchased from EMF Corp. (Ithaca, NY). Pluronic F-108 (a neutral difunctional block copolymer surfactant) was purchased from BASF (Ludwingshafen, Germany). The background electrolyte for all experiments, 5.0 mM Tris-HCl buffer (pH = 8.1), was prepared by diluting 1.0 M Tris-HCl (Fisher Biotech, Fair Lawn, NJ) with deionized water (18 MΩ·cm, Milli-Q Gradient System, Millipore, Bedford, MA). Photoresist (AZ 4620) and developer (AZ 421 K) were obtained from AZ Electronic Materials (Somerville, NJ). Photoresist SU-8 2025 was purchased from MicroChem (Newton, MA). Propylene glycol methyl ether acetate (PGMEA) was obtained from Sigma Aldrich (St. Louis, MO). Isopropyl alcohol, sulfuric acid (H$_2$SO$_4$), and hydrogen peroxide (H$_2$O$_2$) where purchased from Thermo Fisher Scientific (Lair Lawn, NJ). Silicon wafers were obtained from University Wafer, Inc. (Boston, MA).

Microfluidic device fabrication

All BPEs and driving electrodes were patterned on Au-coated glass slides using standard photolithographic techniques.[25] The BPE masks and microchannel masters were designed using CorelDRAW Graphics Suite 12 and printed by CAD/Art Services, Inc. (Bandon, OR). The Y-shaped microchannels used in all experiments had dimensions of 3 mm × 100 μm × 22 μm ($l \times w \times h$) for the primary microchannel and 3 mm × 75 μm × 22 μm ($l \times w \times h$) for the secondary microchannels. Gold driving electrodes, used to apply a driving potential (E_{tot}), were fabricated on the glass baseplate at the bottom of the PDMS reservoirs. They were connected to a power source via copper wires.

The microchannels were formed by pouring PDMS onto a microchannel master[26] and then curing for 2 h at 65 °C. Briefly, a silicon wafer (1 × 2 in) was cleaned with piranha solution (H$_2$SO$_4$ to H$_2$O$_2$ ratio of 3 : 1) for 10 min prior to use and thoroughly washed with deionized water to remove the excess acid. The wafer was then placed on a spin coater (Laurell Technologies Spincoater) and 1 mL of SU-8 2025 photoresist was added to the top of the wafer. The spin coater was programmed to give ⩽20 μm thick channels as follows: spin at 500 rpm for 10 s, 3500 rpm for 60 s, and then 500 rpm for 10 s. Once the program was completed, the modified wafer was soft baked on a hot plate at 65 °C for 2 min and then at 95 °C for 5 min. Next, a negative channel mask (designed with Corel Draw Suite 12 and printed by CAD/Art Services, Inc.) was placed on top of the baked photoresist and exposed to UV light for 20 s at 150 mJ cm^{-2} via a mask aligner (Suss MA6 Mask Aligner). After UV exposure, the wafer was placed on a hot plate at 65 °C for 1 min and then at 95 °C for 5 min. Finally, the microchannel features on the wafer were developed by submerging the wafer in PGMEA solution for 4–5 min (or until the features were clearly developed). After development, the wafer was rinsed with isopropyl alcohol for 10 s, and then rinsed with deionized water. The wafer was then dried and hard baked at 180 °C for 5 min.

Reservoirs were added to the channel using a 4 mm diameter metallic hole puncher. The glass slide (with the previously patterned BPEs and driving electrodes) and PDMS were placed in vacuum for 2 min and then treated with an O$_2$ plasma for 15 s on the medium power setting (60 W, model

PDC-32G, Harrick Scientific, Ossining, NY). Immediately after exposure to the plasma, the glass slide and PDMS were pressed together and placed in the oven at 65 °C for 5 min. When removed from the oven, the microchannels were immediately filled with buffer solution. All devices were coated with Pluronic F-108 by placing one pellet inside the anodic reservoir and flowing buffer over it for 30 min prior to experiments.[27,28] This step was carried out to minimize the electroosmotic flow (EOF) produced upon the application of a potential bias.[29,30] By doing so, the electric field is lengthened, which results in enhanced enrichment and improved separation resolution (i.e., narrower enriched bands). After coating, the microchannels were rinsed twice for 5 min using fresh buffer solution.

Data acquisition and instrumentation

Fluorescence micrographs were obtained using a Nikon AZ100 (Nikon Co., Tokyo, Japan) microscope equipped with a mercury lamp (Nikon) and a CCD camera (Cascade, Photometrics Ltd., Tucson, AZ). All images were captured using 1×1 binning with 512×290 pixels and a 1.00 s exposure time. Fluorescence micrographs were processed using V^{++} Precision Digital Imaging software (Digital Optics, Auckland, New Zealand). All movies (.AVI, provided in the Electronic Supplementary Information (ESI†)) were created by compiling consecutive frames with the aid of ImageJ 1.45s software at a rate of 4 frames per s. False color was added using the V^{++} software to enhance the visual difference between the enriched bands (Fig. S1, ESI†). The background was colored white, while BODIPY^{2-} and MPTS^{3-} were colored green and blue, respectively. Brightness and contrast of all fluorescence micrographs and movies were manipulated to enhance visualization of the different enriched bands; however, the unadulterated images are provided in Fig. S2 and S3 in the ESI.†

Gating experiments

For all experiments, the following initial conditions were used: E_{tot} = 30.0 V, the buffer solution was 5.0 mM Tris-HCl (pH = 8.1), and the initial concentrations of BODIPY^{2-} and MPTS^{3-} were 1.0 and 15.0 μM, respectively. A higher initial MPTS^{3-} concentration was required because the filter used to track the dye (see ESI†) did not exactly match the range of excitation and emission wavelengths of the molecule (λ_{ex} = 454 nm and λ_{em} = 511 nm). The BPEs used were defined by connecting two 20 μm-long microbands external to the fluidic channels (Fig. 2g). The effective lengths of the split BPEs depend on the distance between the outer edges of pairs of microbands.[30–33] Switching between BPEs was performed using a custom switch box.

Measurement of analyte leakage into the gated secondary microchannels

The individual frames of Movies S1 and S2, ESI† were analyzed to quantify the relative amount of analyte that leaked into the gated secondary microchannel during each experiment. This was done by comparing a frame from the movie captured before analyte delivery with one captured during delivery of the analyte, and measuring the fluorescence intensity at the same point in the gated secondary microchannel (where analyte entry is undesirable). The original movie frames used

to measure the leakage of analytes are provided in Fig. S4 and S5, ESI† for the main and alternative BPE configuration, respectively.

Results and discussion

Principles of electrochemically-gated delivery

In recent years, we have reported on the theory[23,30,31,34,35] and some interesting applications[23,36–44] of bipolar electrochemistry. Two important applications of bipolar electrochemistry that are particularly relevant to the present report are analyte enrichment[30,31,34,35,45,46] and separation.[29] However, the principles underpinning all of these methods are similar. Specifically, when a potential (E_{tot}) is applied across a buffer-filled microfluidic channel, an electric field forms. If a conductive substrate, the BPE in this case, is present within the channel, then the potential between the two poles of the BPE and the solution will be different (Fig. 2a). The potential dropped across the length of the BPE (ΔE_{elec}) depends on E_{tot} and the length of the BPE (l_{elec}). If ΔE_{elec} is sufficiently large, then faradaic reactions will occur at the BPE poles. In the present case, water is reduced at the cathodic pole to yield OH$^-$ (Fig. 2c). If the buffer solution contains an acid (e.g., TrisH$^+$), electrogenerated OH$^-$ will partially neutralize the buffer solution (Fig. 2c) creating a region depleted of charge. This loss of ionic charge carriers results in increased resistance near the BPE cathode and a corresponding local field gradient (solid blue line in Fig. 2b).

Because the velocity of electromigration (v_m) is proportional to electric field strength, charged analytes migrate faster in the depletion zone. However, this local velocity increase is opposed by the velocity of convection (v_{conv}, consisting of EOF and PDF), which is nearly uniform throughout the microchannel due to the incompressibility of water. Therefore, at the location on the electric field gradient where v_m and v_{conv} are equal in magnitude and opposite in direction, enrichment occurs (Fig. 2b). Because v_m depends on electrophoretic mobility (μ_{ep}), species having different μ_{ep} can be separated into distinct enriched bands at different points on the electric field gradient.[29]

Operation of electrochemical gates

Electrochemical gating is a consequence of the principles discussed in the previous section. Upon application of an appropriate voltage (E_{tot}) across the Y-shaped channel shown in Fig. 1, and in the presence of a BPE, charged analytes are enriched and separated in the primary channel at positions that depend on their electrokinetic and convective velocities. After enrichment and separation, additional BPEs can be activated or deactivated to guide the enriched analytes into secondary channels (SC1 and SC2, Fig. 1).

The BPEs used in the present report are split.[30–33,47] Split, or discontinuous, BPEs (Fig. 2g and 2h) differ from continuous BPEs (Fig. 2f) in that they can be switched between active and inactive states by connecting or disconnecting, respectively, two separate microbands. Here, activation means that faradaic reactions occur at the two poles of the BPE. Three separate
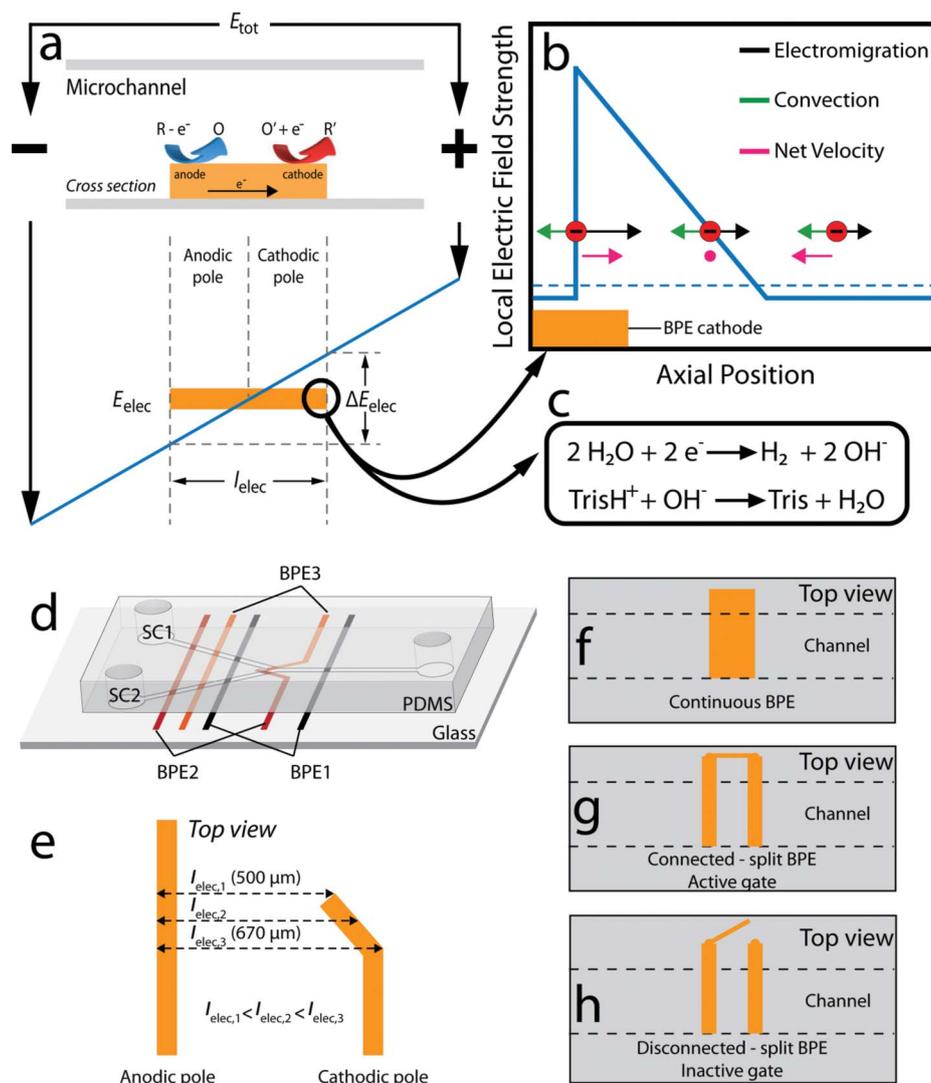
Fig. 2 (a) Illustration of the underlying principles governing bipolar electrochemistry. (b) A schematic representation showing how balancing of electromigration and convection lead to enrichment. (c) Electrochemical reactions taking place at the cathodic pole of the BPE. (d) A three-dimensional view of the device used to obtain the data shown in Fig. 3. (e) A close-up representation of the design of BPE2 and BPE3 showing how the BPE length is a function of location. (f) Representation of a continuous BPE. (g) Representation of a split BPE when it is connected (active gate). (h) Representation of a split BPE when it is disconnected (inactive gate).

split BPEs (BPE1, BPE2, and BPE3, Fig. 2d) are required to achieve permanent separation of two enriched dyes into each of two secondary microchannels.

Fig. 3 shows the actual operation of a BPE gating device like the one illustrated in Fig. 2d. The cathodic pole of BPE1 (black BPE in Fig. 3a and 3b) extends across the entire width of the primary microchannel so it can be used for enrichment and separation of analytes in the primary microchannel before gating begins. BPE2 and BPE3 (red and orange BPEs in Fig. 3c and 3d, respectively) are used to control analyte delivery to the secondary microchannels, and hence their cathodic poles are placed at the intersections of the primary and secondary microchannels. Experiments carried out using different BPE orientations (discussed later) showed that the angled geometry of BPE2 and BPE3 (cathodic poles are perpendicular to the secondary microchannel being gated (blocked)) is more

effective for guiding the movement of the enriched bands into the desired secondary microchannels. This expectation is justified, because the magnitude of ΔE_{elec} increases with BPE length (Fig. 2a); therefore, the rate of the buffer neutralization reaction is greatest when the separation between the poles is greatest. This point is clearly illustrated in Fig. 2e, which shows how the effective lengths of BPE2 and BPE3 vary depending on the distance between their anodic and cathodic poles. As shown in the figure, the electric field strength follows the order $l_{elec,1} < l_{elec,2} < l_{elec,3}$. The key point is that BPE2 and BPE3 guide the enriched bands into the target secondary microchannel by creating a progressively decreasing electric field strength.

The experiment shown in Fig. 3 was carried out as follows (note that the frames in this figure were extracted from Movie S1 in the ESI†). First, the poles of BPE1 were connected and a
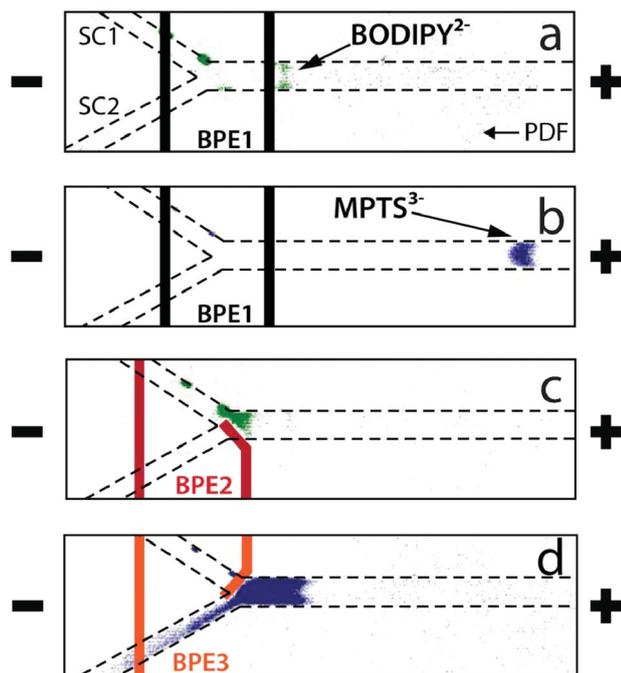
Fig. 3 Enrichment, separation, and selective transport of BODIPY^{2-} and MPTS^{3-} (green and blue, respectively). The black, red, and orange pairs of solid lines represent the location of the microbands that form active BPEs during each stage of the experiment, and the black dashed lines show the locations of the microchannels. The plus and minus signs represent the anodic and cathodic reservoirs, respectively. The Tris-HCl buffer concentration was 5.0 mM (pH = 8.1) and E_{tot} = 30.0 V. Enrichment and separation of (a) BODIPY^{2-} and (b) MPTS^{3-} using BPE1 (black BPE). The enrichment step (BPE1 active) was carried out for ~28 s. (c) Transport of BODIPY^{2-} into SC1 after activation of BPE2 (red BPE). (d) Transport of MPTS^{3-} into SC2 after activation of BPE3 (orange BPE). Note that BODIPY^{2-} and MPTS^{3-} were imaged using different optical filters, which meant that both bands could not be imaged simultaneously.

voltage of E_{tot} = 30.0 V was applied between the driving electrodes. As shown in Fig. 3, this results in enrichment and separation of BODIPY^{2-} (Fig. 3a) and MPTS^{3-} (Fig. 3b) in the primary channel.[29,48,49] Note that different fluorescence filters were used to detect the two tracers. Second, BPE1 was deactivated at the same time that BPE2 (Fig. 3c, red BPE) was activated. The activation of only BPE2 results in the opening of the electrochemical gate at the entrance of SC1. Now, when the PDF is increased slightly by addition of 1.0 μL of buffer to the anodic reservoir, the BODIPY^{2-} band is delivered into SC1. Third, BPE2 was deactivated while simultaneously activating BPE3 (Fig. 3d, orange BPE). This results in collapse of the electric field gradient near the entrance to SC2. However, activation of BPE3 results in an equivalent electric field gradient in front of SC1. By again increasing the PDF toward the cathodic reservoirs (by addition of a total of 5.0 μL of buffer solution to the anodic reservoir), the enriched MPTS^{3-} band moves into SC2. Note that because MPTS^{3-} has a higher μ_{ep} than BODIPY^{2-}, a higher convective velocity is required to push the enriched band out of the primary microchannel and into SC2. These results demonstrate that a simple set of BPEs and a single DC power supply

can be used to separate, enrich, and then permanently separate the two tracers.

Quantitative evaluation of electrochemical gates

As discussed in the previous section, the progressive electric field gradient is created by the orientation of the cathodic poles of BPE2 and BPE3, and it is responsible for the clean delivery of the enriched bands into the proper secondary microchannels. As shown in Fig. S1 and S4 in the ESI,† there is no detectable leakage of the analytes outside the microchannels or into the wrong secondary microchannels, respectively. Additionally, BPE gating is highly reproducible. That is, the success rate for delivering 100% of the correct enriched bands into the correct secondary microchannels using two independently fabricated microfluidic devices (with two trials for each device) was 100%. Note, however, that at enrichment times >30 s (with BPE1 active) the MPTS^{3-} band was sometimes observed to move backwards into the anodic reservoir when BPE1 and BPE2 were switched off and on, respectively. This observation is a consequence of the larger ΔE_{elec} arising from the angled geometry of the gating BPEs (BPE2 in this case) compared to BPE1. Accordingly, the total enrichment time allotted in these experiments (while BPE1 was active) was limited to ~30 s. One final point: even though the purpose of BPE2 and BPE3 is to deliver the enriched bands into the secondary microchannels, enrichment continues whenever they are active.

We have previously defined a parameter called the enrichment factor (EF), which is used for benchmarking the extent of BPE-driven analyte concentration. The EF is defined as the concentration of the enriched tracer (determined using a calibration curve of fluorescence intensity $vs.$ concentration of dye) measured at a specific time during an experiment, divided by its original concentration. In earlier reports from our lab, where the objective was to maximize the EF using the same general approach described here, we reported EFs of up to 500 000.[49] However, in the present case (Fig. 3) the EFs were much lower: BODIPY^{2-} 3.1 ± 0.1 after 26 s; and MPTS^{3-} 27 ± 2 after 56 s. These EFs were calculated using the calibration curves shown in Fig. S6, ESI.† These low values are primarily a consequence of the short time allotted for enrichment in these experiments. Note, however, that the rates of enrichment of both dyes (0.11-fold/s and 0.31-fold/s for BODIPY^{2-} and MPTS^{3-}, respectively) are comparable to those we reported previously (0.57 and 0.75 fold/s)[29,30] and that resulted in much higher total EFs. Importantly, they are also comparable to those obtained using EFGF (4.0 fold/s),[19] when differences in the experimental conditions are taken into account.

Fig. 4 shows the measured fluorescence intensity in the primary microchannel throughout the course of the experiment represented by the snapshots in Fig. 3 and shown explicitly in Movie S1, ESI.† The BODIPY^{2-} enriched band experienced an increase in fluorescence intensity between 0 and 40 s. At t = 30 s the gate defined by BPE1 was opened, and at t = 40 s the enriched BODIPY^{2-} band was guided into SC1 and completely removed from the primary microchannel. This resulted in an immediate decrease in fluorescence intensity. The MPTS^{3-} fluorescence intensity also increased during the initial 40 s, but as the BODIPY^{2-} band moved out of the primary microchannel (t = 40 s) the MPTS^{3-} fluorescence
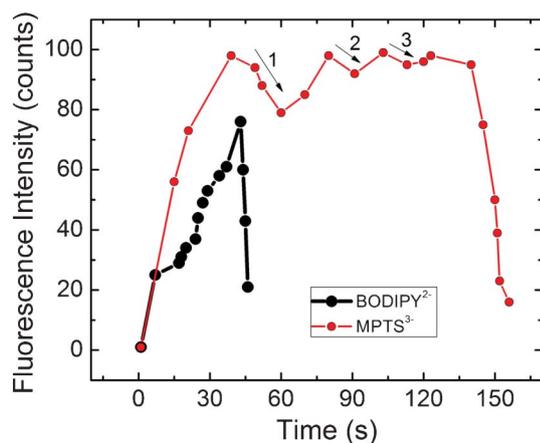
Fig. 4 Plot of fluorescence intensity measured in the primary microchannel for $BODIPY^{2-}$ and $MPTS^{3-}$ throughout the course of the experiment shown in Fig. 3 and Movie S1, ESI.† The black arrows indicate a decrease in fluorescence intensity when PDF was increased towards the cathodic reservoirs.

Fig. 5 Alternative BPE configuration for the enrichment, separation, and controlled delivery of $BODIPY^{2-}$ and $MPTS^{3-}$. The black and red pairs of solid lines represent the location of the microbands that form active BPEs during each stage of the experiment, and the black dashed lines represent the locations of the microchannels. The plus and minus signs represent the anodic and cathodic reservoirs, respectively. The Tris-HCl buffer concentration was 5.0 mM (pH = 8.1) and E_{tot} = 30.0 V. Enrichment and separation of (a) $BODIPY^{2-}$ and (b) $MPTS^{3-}$; (c) transport of $BODIPY^{2-}$ into SC2; and (d) transport of $MPTS^{3-}$ into SC1.

intensity temporarily decreased slightly (arrow 1 in Fig. 4). This is because as soon as the $BODIPY^{2-}$ band is delivered into SC1, 3.0 µL of buffer solution were added to the anodic reservoir to move the enriched $MPTS^{3-}$ band toward SC2. This change in v_{conv} temporarily disrupts the conditions required for $MPTS^{3-}$ enrichment, slightly dispersing the enriched band and decreasing the fluorescence intensity. As additional 1.0 µL aliquots of buffer are added to the anodic reservoir, to push the $MPTS^{3-}$ band further towards SC2 (indicated by arrows 2 and 3), two additional temporary decreases in fluorescence are observed for the same reason. Finally, the $MPTS^{3-}$ fluorescence intensity abruptly decreases when the enriched band is guided into SC2 at t = 140 s.

Alternative BPE configuration

The desirable characteristics of the BPE design described in the previous sections are: simultaneous enrichment and separation of a mixture of two charged dyes, robust control over the delivery of the enriched bands into the desired secondary microchannel, and no leakage of enriched bands into the untargeted secondary microchannel during delivery. However, this design also has some limitations. For example, due to the positioning of BPE2 and BPE3 in the primary microchannel, it is only useful for permanent separation of two analytes. A configuration that resolves this problem is shown in Fig. 5. Here, both halves of the split BPEs are placed within the secondary microchannels, so that many secondary channels, and hence many analytes, could be permanently separated. In the experiment discussed next, we demonstrate the principle using just two secondary channels.

The experiment is initiated by applying E_{tot} = 30.0 V between the driving electrodes. To induce enrichment and separation, both BPEs are simultaneously activated (Fig. 5a and 5b). In effect, these two BPEs act as a single BPE spanning the width of the primary microchannel. As a consequence, $BODIPY^{2-}$ and $MPTS^{3-}$ form resolved and enriched bands in the primary microchannel (with EFs of 3.4 ± 0.1 for $BODIPY^{2-}$ after 20 s and 12.9 ± 0.9 for $MPTS^{3-}$ after 49 s).

Following enrichment and separation, the red BPE is disconnected (Fig. 5c) and simultaneously the PDF is increased in the direction of the cathodic reservoirs by adding 1.0 µL of buffer to the anodic reservoir. This results in transport of the enriched $BODIPY^{2-}$ into SC2. Once the $BODIPY^{2-}$ band is completely removed from the primary microchannel, the red BPE is reconnected to prevent passage of the enriched $MPTS^{3-}$ band into SC2. Next, PDF is further increased by adding another 1.0 µL aliquot of buffer to the anodic reservoir. This results in an increase in v_{conv}, thereby driving $MPTS^{3-}$ down the primary microchannel in the direction of the cathodic reservoirs. As the $MPTS^{3-}$ band approaches the microchannel intersection, the black BPE is disconnected, allowing $MPTS^{3-}$ to flow into SC1 (Fig. 5d). A movie (Movie S2, ESI†) showing the experiment from which the frames in Fig. 5a–5d were obtained is provided in the ESI.†

Fig. S5 (ESI†) demonstrates that there is no detectable leakage of $BODIPY^{2-}$ or $MPTS^{3-}$ into the untargeted secondary microchannels during the gating process shown in Fig. 5. However, we tested 10 independently prepared devices having this alternative design, and the device-to-device success rate for delivering 100% of the correct enriched bands into the correct secondary channels was just 37%. This relatively low

value arises from broadening of the enriched bands at the microchannel intersection, which in turn arises from the difficulty of reproducibly increasing v_{conv} for this particular configuration.

Summary and conclusions

Fluidic handling on the microscale usually involves integrated combinations of on-chip valves, pumps, dams, membranes, and separators, and due to the complexity of their fabrication and need to synchronize their operation it is desirable to consider simpler approaches. The method described here coordinates the operations of enrichment, separation, and selective, controlled delivery using just electric field manipulation and very slight variations in PDF. Device fabrication is likewise very simple: it only requires integration of BPEs and an external low-voltage DC power supply.

We believe the fluidic handling techniques presented here could be automated so as to be coupled to other quantitative techniques, such as mass spectrometry or gel electrophoresis, and this is one of the goals of our future work. We also plan to expand the scope of the work to include separation of mixtures of proteins and improved EFs. These goals can be achieved by increasing the enrichment time and buffer concentration,[30] decreasing the cross-sectional area of the channel,[49] increasing the electric field, decreasing the initial concentration of the analyte,[30] and increasing the length of the primary channel. Experiments and simulations demonstrating these findings will be reported in due course.

Acknowledgements

References

1 G. S. Fiorini and D. T. Chiu, Disposable Microfluidic Devices: Fabrication, Function, and Application, *BioTechniques*, 2005, **38**, 429–446.

2 A. Y. Fu, H.-P. Chou, C. Spence, F. H. Arnold and S. R. Quake, An Integrated Microfabricated Cell Sorter, *Anal. Chem.*, 2002, **74**, 2451–2457.

3 V. Bahadur and S. V. Garimella, Electrical Actuation-Induced Droplet Transport on Smooth and Superhydrophobic Surfaces, *Int. J. Micro-Nano Scale Transp.*, 2010, **1**, 1–26.

4 D. Chugh and K. V. I. S. Kaler, Leveraging Liquid Dielectrophoresis for Microfluidic Applications, *Biomed. Mater.*, 2008, **3**, 034009.

5 H. Tan and E. S. Yeung, Automation and Integration of Multiplexed On-Line Sample Preparation with Capillary Electrophoresis for High-Throughput DNA Sequencing, *Anal. Chem.*, 1998, **70**, 4044–4053.

6 M. C. Weston, M. D. Gerner and I. Fritsch, Magnetic Fields for Fluid Motion, *Anal. Chem.*, 2010, **82**, 3411–3418.

7 F. M. Weinert, C. B. Mast and D. Braun, Optical Fluid and Biomolecule Transport with Thermal Fields, *Phys. Chem. Chem. Phys.*, 2011, **13**, 9918–9928.

8 B. S. Gallardo, V. K. Gupta, F. D. Eagerton, L. I. Jong, V. S. Craig, R. R. Shah and N. L. Abbott, Electrochemical Principles for Active Control of Liquids on Submillimeter Scales, *Science*, 1999, **283**, 57–60.

9 D. E. Kataoka and S. M. Troian, Patterning Liquid Flow on the Microscopic Scale, *Nature*, 1999, **402**, 794–797.

10 J. Friend and L. Y. Yeo, Microscale Acoustofluidics: Microfluidics Driven Via Acoustics and Ultrasonics, *Rev. Mod. Phys.*, 2011, **83**, 647–704.

11 C. Liu, Y. Luo, E. J. Maxwell, N. Fang and D. D. Y. Chen, Reverse of Mixing Process with a Two-Dimensional Electro-Fluid-Dynamic Device, *Anal. Chem.*, 2010, **82**, 2182–2185.

12 J. G. Shackman and D. Ross, Counter-flow gradient electrofocusing, *Electrophoresis*, 2007, **28**, 556–571.

13 W. S. Koegler and C. F. Ivory, Focusing proteins in an electric field gradient, *J. Chromatogr., A*, 1996, **726**, 229–236.

14 W. S. Koegler and C. F. Ivory, Field Gradient Focusing: A Novel Method for Protein Separation, *Biotechnol. Prog.*, 1996, **12**, 822–836.

15 R. T. Kelly and A. T. Woolley, Electric field gradient focusing, *J. Sep. Sci.*, 2005, **28**, 1985–1993.

16 X. Sun, P. B. Farnsworth, H. D. Tolley, K. F. Warnick, A. T. Woolley and M. L. Lee, Performance optimization in electric field gradient focusing, *J. Chromatogr., A*, 2009, **1216**, 159–164.

17 X. Sun, D. Li, A. T. Woolley, P. B. Farnsworth, H. D. Tolley, K. F. Warnick and M. L. Lee, Bilinear electric field gradient focusing, *J. Chromatogr., A*, 2009, **1216**, 6532–6538.

18 S.-L. Lin, Y. Li, A. T. Woolley, M. L. Lee, H. D. Tolley and K. F. Warnick, Programed elution and peak profiles in electric field gradient focusing, *Electrophoresis*, 2008, **29**, 1058–1066.

19 P. H. Humble, R. T. Kelly, A. T. Woolley, H. D. Tolley and M. L. Lee, Electric Field Gradient Focusing of Proteins Based on Shaped Ionically Conductive Acrylic Polymer, *Anal. Chem.*, 2004, **76**, 5641–5648.

20 S.-L. Lin, Y. Li, H. D. Tolley, P. H. Humble and M. L. Lee, Tandem electric field gradient focusing system for isolation and concentration of target proteins, *J. Chromatogr., A*, 2006, **1125**, 254–262.

21 D. N. Petsev, G. P. Lopez, C. F. Ivory and S. S. Sibbett, Microchannel protein separation by electric field gradient focusing, *Lab Chip*, 2005, **5**, 587–597.

22 L. Bouffier and A. Kuhn, Design of a wireless electrochemical valve, *Nanoscale*, 2013, **5**, 1305–1309.

23 F. Mavré, R. K. Anand, D. R. Laws, K.-F. Chow, B.-Y. Chang, J. A. Crooks and R. M. Crooks, Bipolar Electrodes: A Useful Tool for Concentration, Separation, and Detection of Analytes in Microelectrochemical Systems, *Anal. Chem.*, 2010, **82**, 8766–8774.

24 G. Loget and A. Kuhn, Shaping and Exploring the Micro-and Nanoworld Using Bipolar Electrochemistry, *Anal. Bioanal. Chem.*, 2011, **400**, 1691–1704.

25 Y. Xia and G. M. Whitesides, Soft Lithography, *Angew. Chem., Int. Ed.*, 1998, **37**, 550–575.

26 J. C. McDonald, D. C. Duffy, J. R. Anderson, D. T. Chiu, H. Wu, O. J. A. Schueller and G. M. Whitesides, Fabrication of Microfluidic Systems in Poly(dimethylsiloxane), *Electrophoresis*, 2000, **21**, 27–40.

27 E. A. S. Doherty, R. J. Meagher, M. N. Albarghouthi and A. E. Barron, Microchannel Wall Coatings for Protein Separations by Capillary and Chip Electrophoresis, *Electrophoresis*, 2003, **24**, 34–54.

28 W. Hellmich, J. Regtmeier, T. T. Duong, R. Ros, D. Anselmetti and A. Ros, Poly(oxyethylene) Based Surface Coatings for Poly(dimethylsiloxane) Microchannels, *Langmuir*, 2005, **21**, 7551–7557.

29 D. R. Laws, D. Hlushkou, R. K. Perdue, U. Tallarek and R. M. Crooks, Bipolar Electrode Focusing: Simultaneous Concentration Enrichment and Separation in a Microfluidic Channel Containing a Bipolar Electrode, *Anal. Chem.*, 2009, **81**, 8923–8929.

30 R. K. Anand, E. Sheridan, D. Hlushkou, U. Tallarek and R. M. Crooks, Bipolar Electrode Focusing: Tuning the Electric Field Gradient, *Lab Chip*, 2011, **11**, 518–527.

31 R. K. Perdue, D. R. Laws, D. Hlushkou, U. Tallarek and R. M. Crooks, Bipolar Electrode Focusing: The Effect of Current and Electric Field on Concentration Enrichment, *Anal. Chem.*, 2009, **81**, 10149–10155.

32 A. Arora, J. C. T. Eijkel, W. E. Morf and A. Manz, A Wireless Electrochemiluminescence Detector Applied to Direct and Indirect Detection for Electrophoresis on a Microfabricated Glass Device, *Anal. Chem.*, 2001, **73**, 3282–3288.

33 F. Mavré, K.-F. Chow, E. Sheridan, B.-Y. Chang, J. A. Crooks and R. M. Crooks, A Theoretical and Experimental Framework for Understanding Electrogenerated Chemiluminescence (ECL) Emission at Bipolar Electrodes, *Anal. Chem.*, 2009, **81**, 6218–6225.

34 D. Hlushkou, R. K. Perdue, R. Dhopeshwarkar, R. M. Crooks and U. Tallarek, Electric Field Gradient Focusing in Microchannels with Embedded Bipolar Electrode, *Lab Chip*, 2009, **9**, 1903–1913.

35 R. Dhopeshwarkar, D. Hlushkou, M. Nguyen, U. Tallarek and R. M. Crooks, Electrokinetics in Microfluidic Channels Containing a Floating Electrode, *J. Am. Chem. Soc.*, 2008, **130**, 10480–10481.

36 E. Sheridan, K. N. Knust and R. M. Crooks, Bipolar Electrode Depletion: Membraneless Filtration of Charged Species Using an Electrogenerated Electric Field Gradient, *Analyst*, 2011, **136**, 4134–4137.

37 S. E. Fosdick and R. M. Crooks, Bipolar Electrodes for Rapid Screening of Electrocatalysts, *J. Am. Chem. Soc.*, 2012, **134**, 863–866.

38 B.-Y. Chang, F. Mavré, K.-F. Chow, J. A. Crooks and R. M. Crooks, Snapshot Voltammetry Using a Triangular Bipolar Microelectrode, *Anal. Chem.*, 2010, **82**, 5317–5322.

39 K.-F. Chow, B.-Y. Chang, B. A. Zaccheo, F. Mavré and R. M. Crooks, A Sensing Platform Based on Electrodissolution of a Ag Bipolar Electrode, *J. Am. Chem. Soc.*, 2010, **132**, 9228–9229.

40 K.-F. Chow, F. Mavré and R. M. Crooks, Wireless Electrochemical DNA Microarray Sensor, *J. Am. Chem. Soc.*, 2008, **130**, 7544–7545.

41 I. Dumitrescu, R. K. Anand, S. E. Fosdick and R. M. Crooks, Pressure-Driven Bipolar Electrochemistry, *J. Am. Chem. Soc.*, 2011, **133**, 4687–4689.

42 W. Zhan, J. Alvarez and R. M. Crooks, A Two-channel Microfluidic Sensor that Uses Anodic Electrogenerated Chemiluminescence as a Photonic Reporter of Cathodic Redox Reactions, *Anal. Chem.*, 2003, **75**, 313–318.

43 W. Zhan, J. Alvarez, L. Sun and R. M. Crooks, A Multichannel Microfluidic Sensor that Detects Anodic Redox Reactions Indirectly Using Anodic Electrogenerated Chemiluminescence, *Anal. Chem.*, 2003, **75**, 1233–1238.

44 W. Zhan and R. M. Crooks, Microelectrochemical Logic Circuits, *J. Am. Chem. Soc.*, 2003, **125**, 9934–9935.

45 E. Sheridan, D. Hlushkou, K. N. Knust, U. Tallarek and R. M. Crooks, Enrichment of Cations via Bipolar Electrode Focusing, *Anal. Chem.*, 2012, **84**, 7393–7399.

46 K. N. Knust, E. Sheridan, R. K. Anand and R. M. Crooks, Dual-channel bipolar electrode focusing: simultaneous separation and enrichment of both anions and cations, *Lab Chip*, 2012, **12**, 4107–4114.

47 W. Zhan, J. Alvarez and R. M. Crooks, Electrochemical Sensing in Microfluidic Systems Using Electrogenerated Chemiluminescence as a Photonic Reporter of Redox Reactions, *J. Am. Chem. Soc.*, 2002, **124**, 13265–13270.

48 E. Sheridan, D. Hlushkou, R. K. Anand, D. R. Laws, U. Tallarek and R. M. Crooks, Label-Free Electrochemical Monitoring of Concentration Enrichment during Bipolar Electrode Focusing, *Anal. Chem.*, 2011, **83**, 6746–6753.

49 R. K. Anand, E. Sheridan, K. N. Knust and R. M. Crooks, Bipolar Electrode Focusing: Faradaic Ion Concentration Polarization, *Anal. Chem.*, 2011, **83**, 2351–2358.